A theoretical insight into the catalytic effect of a mixed-metal oxide at the nanometer level: The case of the highly active $\mathrm{metal/CeO}_x/\mathrm{TiO}_2(110)$ catalysts

Jesús Graciani, José J. Plata, Javier Fdez. Sanz, Ping Liu, and José A. Rodriguez

View Online   Export Citation

ARTICLES YOU MAY BE INTERESTED IN

A theoretical insight into the catalytic effect of a mixed-metal oxide at the nanometer level: The case of the highly active metal/CeO$_x$/TiO$_2$(110) catalysts

Jesús Graciani,[1,2,a)] José J. Plata,[2] Javier Fdez. Sanz,[2] Ping Liu,[1] and José A. Rodriguez[1]
[1]*Department of Chemistry, Brookhaven National Laboratory, Upton, New York 11973, USA*
[2]*Departamento de Química Física, Facultad de Química, Universidad de Sevilla, Sevilla E-41012, Spain*

The structural and electronic properties of CeO$_x$ species supported on the rutile TiO$_2$(110) surface have been examined by means of periodic density-functional calculations that use a generalized gradient approximation functional including a Hubbard-like type correction. Deposition of Ce atoms leads in a first step to Ce^{3+} ions bound to the surface through bridge and in-plane oxygen atoms, the released electrons occupying the Ti 3d empty orbitals. Further addition of Ce and molecular oxygen gives place to Ce$_2$O$_3$ dimers diagonally arranged on the surface, in agreement with the spots observed in the scanning tunnel microscope images. The formation process of CeO$_x$ nanoparticles (NPs) on the TiO$_2$ surface is highly exothermic and our calculations show that the redox properties of the Ce(III)-Ce(IV) couple are significantly altered when it is supported on TiO$_2$. In particular the reactivity against CO/O$_2$ indicates that on the surface the presence of Ce(III) is favored over Ce(IV) species. Our results also indicate that the CeO$_x$/TiO$_2$ interface should be seen like a real mixed-metal oxide rather than a supported NP of ceria. Finally, in the context of the high catalytic activity of the M/CeO$_x$/TiO$_2$ (M = Au, Cu, Pt) systems in the water-gas shift reaction, we have examined the dissociation of water on the CeO$_x$/TiO$_2$ surface and estimated a barrier as small as 0.04 eV, i.e. ~8 times smaller than that computed for a TiO$_2$ oxygen vacancy. This result agrees with the experimental superior catalytic activity of the M/CeO$_x$/TiO$_2$ systems over M/TiO$_2$. © *2010 American Institute of Physics.* [doi:10.1063/1.3337918]

I. INTRODUCTION

Catalytic processes able to reduce the environmental pollution or generate new clean renewable sources of energy have received an increasing attention and become one of the hot spots in chemistry.[1–5] In this regard, a number of works have been devoted to design new better catalyst intended to eliminate CO, either by plane oxidation $\left(CO + \frac{1}{2}O_2 \rightarrow CO_2\right)$ or further transformation through, for instance, the water gas shift (WGS) reaction, $(CO + H_2O \rightarrow CO_2 + H_2)$, widely used to produce H$_2$ clean enough to be used in fuel cells.[3–7] Many metal/metal-oxide systems have been found to catalyze these important reactions under different conditions, and among them, two of the most efficient systems are based on gold nanoparticles (NPs), supported on a reducible metal oxide such as titania or ceria (Au/TiO$_2$ and Au/CeO$_2$).[3–15] The ability of both systems to easily generate reduced species of Ti and Ce (Ti^{3+}/Ce^{3+}) has been found to play a crucial role on their catalytic activities.[16–19]

In the WGS reaction, previous work performed on a variety of systems such as Au/CeO$_2$, Au/TiO$_2$, Au/TiO$_{2-x}$N$_y$, Cu/TiO$_2$, CeO$_x$/Au(111), CeO$_x$/Cu(111), and Au/CeO$_x$/TiO$_2$, has shown that the main role of the metal is to adsorb CO while the role of the oxide is to dissociate water.[12,20–23] Although all the steps involved in the WGS reaction might occur on the surface of the metal, or metal NP, the high activation barriers estimated for the dissociation of H$_2$O makes the bare metal a quite inefficient catalyst.[24,25] That is why it is critical that the properties of the oxide facilitate H$_2$O dissociation.[20,12] On its turn, metal-oxide surfaces readily adsorb water, and are able to dissociate H$_2$O easily, mainly at the O vacancy sites, to produce hydroxyls that cover the surface. However, in a WGS environment, these hydroxyls usually react with CO to give rise to very stable intermediates (HCOO, CO$_x$) that stop the reaction.[20] Therefore, an adequate combination of the metal oxide and metal properties leads to a high active catalyst: H$_2$O is easily dissociated on the oxide and less stable intermediates which evolve to products with low activation barriers are formed on the metal particle or at the interface.

Oxygen vacancies, which involve the presence of Ti^{3+} or Ce^{3+} species, are the main active sites for dissociative chemisorption of water on TiO$_2$ and CeO$_2$.[20,12,22,26–31] Therefore the presence of reduced species Ti^{3+} or Ce^{3+} is essential to achieve high catalytic activity in the WGS. For instance, a catalyst consisting of CeO$_x$ NPs supported on Au(111) has activities higher than those of standard WGS catalysts such as Cu(111) or Cu(100).[20] The activity was found to be directly related to the presence of some Ce^{3+} species. Another way to enlarge the concentration of active Ce^{3+} sites is to modify the pure oxide by mixing it with a different metal oxide. The properties of these mixed-metal oxides can be very different from those of the pure oxides. Higher effects

a)Author to whom correspondence should be addressed. Electronic mail: graciani@us.es.

can be expected by mixing the oxides at the nanometer level. In fact, in our previous work[21] we have shown that the growing of CeO_x NPs on TiO_2 leads to the formation of some structures of cerium oxide imposed by the interaction with the host oxide in which the relative stability of Ce^{4+}/Ce^{3+} is strongly affected to the point that all Ce atoms are in a +3 oxidation state. Deposition of Au nanoclusters on these mixed metal-oxide CeO_x/TiO_2 surfaces leads to catalysts that show a dramatic improvement in the activity, even larger than that observed for the WGS on $CeO_x/Au(111)$ or Au/CeO_2.[20,21] Extremely high WGS activity is also found for the $Cu/CeO_x/TiO_2(110)$ and $Pt/CeO_x/TiO_2(110)$ systems.[32]

Although a direct influence of the mixed-metal oxide properties on the catalytic activity has been suggested, a detailed analysis of the CeO_x/TiO_2 interface at the electronic level has not yet been reported. For instance, the origin of the predominance of Ce^{3+} over Ce^{4+} species at the surface, or the ability of such a system to dissociate water molecules, still remain open questions. In the present paper we report a theoretical work based on periodic density-functional calculations of the formation process of CeO_x NPs on the TiO_2 surface from the interaction of Ce/TiO_2 with O_2, as well as their redox properties, e.g., their reactions with CO/O_2. We study the relation between the geometrical and electronic structures and their impact on the reactivity. Finally we examine the interaction and dissociation of water on the CeO_x/TiO_2 surface. Since the TiO_{2-x} system has also been found to be a good system for the dissociative chemisorption of water, and the formation of TiO_x species on the surface of TiO_2 from interstitial Ti has been recently shown,[33] we have also performed some calculations for the TiO_x/TiO_2 system in order to compare it with CeO_x/TiO_2.

II. DENSITY-FUNCTIONAL CALCULATIONS

The density functional theory (DFT) calculations were performed using the plane-wave-pseudopotential approach within the projector augmented wave method[34] together with the GGA exchange correlation functional proposed by Perdew *et al.*[35] as implemented in the VASP 4.6 code.[36,37] A plane-wave cutoff energy of 400 eV was used. We treated the Ti $(3s, 3p, 3d, 4s)$, Ce $(4f, 5s, 5p, 5d, 6s)$, and O $(2s, 2p)$ electrons as valence states, while the remaining electrons were kept frozen as core states. To obtain faster convergence, thermal smearing of one-electron states $(k_B T = 0.05$ eV$)$ was allowed using the Gaussian smearing method to define the partial occupancies. We chose a (4×2) surface model with the aim to have isolated CeO_x monomers and dimers on the $TiO_2(110)$ surface. The distance between two nearest Ce_2O_3 dimers was ∼6 Å, which is a reasonable distance with a computationally affordable model. In order to avoid spurious effects due to the finite thickness of the slab representing the surface, we used a recently published model of six layers.[38,39] In this model the two lowest layers were fixed at the optimized atomic bulk positions while atoms in the upper four layers were allowed to relax. This surface model has been shown to minimize the well-known energy oscillations as a function of the number of layers (even-odd) and reaches

convergence for both the geometric and electronic surface structures.[38,39] This surface model, that amounts to 288 atoms, has been successfully used in previous works.[21,22,40,41] The energy was estimated at the gamma point. In order to represent adequately the electronic structure of Ce (in particular the $4f$ level of the Ce^{3+} species) we used the GGA $+U$ formalism. The Hubbard U term was added to the plain GGA functional employing the rotationally invariant approach proposed by Dudarev *et al.*,[42] in which the Coulomb U and exchange J parameters are combined into a single parameter $U_{eff} = U - J$. For Ce we have used the U_{eff} of 4.5 eV which was self-consistently calculated by Fabris *et al.*[43] using the linear-response approach of Cococcioni and de Gironcoli[44] and which is in the range of values usually proposed in the literature (4.5–5.5 eV) for GGA$+U$ calculations.[45–53] For the $3d$ states of Ti we also chose a U_{eff} parameter of 4.5 eV as it reproduces the experimental values of the gap between the Ce^{3+} $4f$ and Ti^{3+} $3d$ levels observed in the valence photoemission spectra of $Ce/TiO_2(110)$ system.[21] Although lower values for U_{eff} have also been proposed for a balanced description of bulk CeO_2 and Ce_2O_3 oxides,[54,55] the set of parameters we have selected allows for a correct description of the gaps observed in the experimental photoemission spectra of our systems consisting of CeO_x clusters supported on the $TiO_2(110)$ surface.[21] Furthermore, the presence of Ce^{3+} species was indicated by a characteristic $4f$ peak in the band gap and later confirmed by the magnetization of the Ce atoms (higher than 0.9 electrons) found in the calculations.

The adsorption energy for a given species X (where X stands for Ce atom, H_2O, CO, etc.) has been calculated as

$$E_{ads}(X) = E(X/TiO_2) - E(X) - E(TiO_2),$$

where $E_{ads}(X)$ is the adsorption energy of X on $TiO_2(110)$, $E(X/TiO_2)$ is the total energy of the system in which X is adsorbed on the $TiO_2(110)$ surface, $E(X)$ is the energy of the isolated X and $E(TiO_2)$ is the energy of the slab model of the surface.

Transitions states have been calculated by using the climbing image (CI) version of the nudged elastic band (NEB) algorithm[56] and in all cases, after a vibrational analysis, a single imaginary frequency has been obtained for these structures. Since these calculations have a huge computational cost in the transitions state searches, the model was reduced to four layers. The reliability of this reduced model was verified by comparing the reaction energy for the water dissociation at the surface from both models: −0.70 eV (six-layer thick model) versus −0.64 eV (four-layer thick model).

III. RESULTS AND DISCUSSION

A. Growth of the CeO_x particles on $TiO_2(110)$

Previous scanning tunneling microscopy (STM) results have shown the formation of CeO_x NPs when depositing Ce on $TiO_2(110)$ in oxygen atmosphere.[21] At low Ce coverage, two kinds of CeO_x spots were identified and assigned to single Ce atoms and Ce–Ce dimers, which were bonded to bridge O atoms. To determine the structure, stability and oxidation state of these species, we have simulated a process of
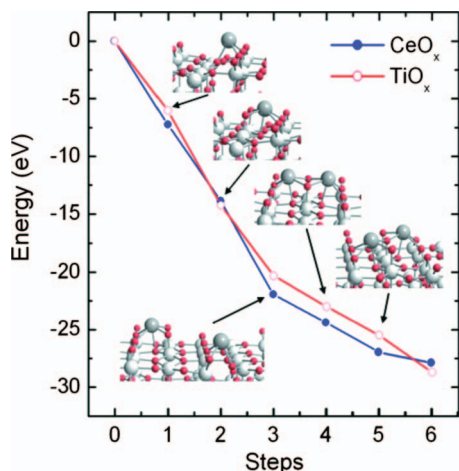
FIG. 1. Energy pathway for the formation of CeO_x and TiO_x species on $TiO_2(110)$ starting from the adsorption of Ce/Ti atoms and subsequent progressive interaction with O_2. M indicates Ce or Ti metal adatoms in each case. Colors: Ce/Ti adatoms (dark gray), Ti atoms of the TiO_2 support (soft gray) and O (soft red). Steps: (1) M atom adsorption, (2) O_2 adsorption-dissociation: formation of the 1st monomer (MO_2), (3) 2nd M atom adsorption, (4) 1st dimer formation (M_2O_2), (5) $(1/2)O_2$ adsorption and 2nd dimer formation (M_2O_3), and (6) $(1/2)O_2$ adsorption and degradation in monomers ($2MO_2$).

sequential adsorption-oxidation for Ce deposited on TiO_2. Figure 1 shows the energy pathway for such a process. The adsorption energy of the first Ce atom is very high (-7.01 eV). On the most stable adsorption site the Ce atom is three-fold coordinated and interacts with one O from the plane and two bridge O (see Fig. 1, step 1). The formal oxidation state is $+3$, which gives rise to the characteristic $4f$ peak above the O $2p$ band on the projected density of states (DOS) (bottom panel in Fig. 2). Upon adsorption, the Ce atom ($6s^25d4f$) formally releases three electrons to the oxide, that are transferred from the Ce $6s$ and $5d$ levels to the lower energy Ti $3d$ states, reducing three Ti atoms to Ti^{3+}. Two of them are
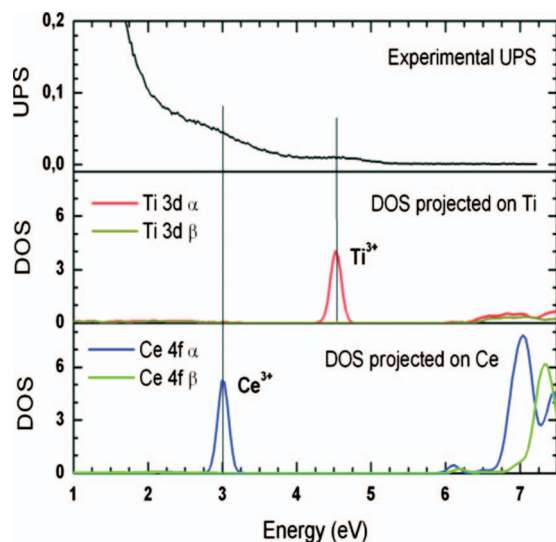

FIG. 2. Experimental photoemission spectrum (top) (Ref. 21), and calculated DOS projected on the reduced Ti atom (middle) and the adsorbed Ce atom (bottom) for the deposition of Ce on $TiO_2(110)$. In the calculation the U_{eff} parameter used for both Ce $4f$ and Ti $3d$ is 4.5 eV. (Reproduced from our previous work in Proc. Natl. Acad. Sci. U.S.A., Ref. 21).

located in the surface layer and the third one is located in the subsurface layer. The fourth valence electron of Ce remains in a $4f$ orbital, whose energy is lower than the empty Ti $3d$ levels (Fig. 2), and therefore is not transferred, leaving the oxidation state of Ce as $+3$. To make a Ce^{4+} ion it would be necessary to have empty states in the O $2p$ band that is lower in energy than the Ce $4f$ level. The high chemisorption energy that we calculated can be understood bearing in mind that there are two complementing contributions to the bond: the large stabilization of the three electrons that shift from high to low energy levels, $Ce(5d6s^2)\rightarrow Ti(3d)$, and the strong electrostatic energy gain that arises from the interaction of the Ce^{3+} cation with three surface O^{2-} anions. Thus, the adsorption process of atomic Ce involves direct bonding with O atoms of the titania and an electron transfer that could be described as

$$Ce + 3Ti^{4+}(TiO_2) \rightarrow Ce^{3+} + 3Ti^{3+}(TiO_2). \qquad (1)$$
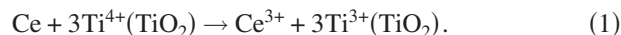
On the other hand, to get Ce^{4+} ions on the stoichiometric oxide would need the presence of extra oxygen. Given that CeO_x species are formed in the presence of O_2,[21] it is appropriate to study the interaction of adsorbed Ce with oxygen. The adsorption-dissociation of O_2 over adsorbed atomic Ce is a highly exothermic process (-6.88 eV). The final structure is a unit of CeO_2 over TiO_2, where the O atoms are adsorbed on the in-plane Ti atoms and strongly interact with the Ce atom that remains in the initial position (see Fig. 1, step 2). This structure is similar to that observed by Wendt *et al.*[33] for interstitial Ti interacting with O_2 on the $TiO_2(110)$ surface. The formal oxidation state of the Ce in this configuration is $+4$. This was neatly observed on the projected DOS on Ce (not shown) where the characteristic $4f$ peak of Ce^{3+} completely disappeared. A further electron rearrangement comes from the fact that to fill the O $2p$ orbitals, in addition to the Ce $4f$, three more electrons are needed, and therefore $3Ti^{3+}$, previously reduced, are reoxidized to Ti^{4+}. This new multielectron transfer, together with the strong electrostatic $Ce^{4+}-O^{2-}$ interaction explain the high energy released in the process, which could be described as
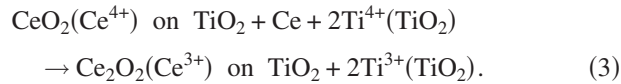
$$Ce^{3+} + 3Ti^{3+}(TiO_2) + O_2 \rightarrow CeO_2(Ce^{4+}) \text{ on } TiO_2. \qquad (2)$$
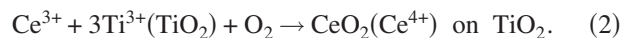
We will call this CeO_2 particle a monomer, which is identified as the small spots observed in STM images for $CeO_x/TiO_2(110)$.[21]

Deposition of the second Ce atom at a surface position far from the monomer (see Fig. 1, step 3) releases an energy of -8.03 eV. As in the case of the first Ce atom, the incoming second Ce atom releases three electrons, one of them does not go to the relatively high energy Ti $3d$ levels, but rather to the lower energy Ce $4f$ of the CeO_2 monomer. Therefore, the Ce^{4+} of the monomer is reduced to Ce^{3+}. If we now move this second Ce atom close to the neighbors of the first Ce atom, there is a release of energy that becomes larger when it is placed in between the two extra O atoms from the CeO_2 monomer and a row of bridge O of the $TiO_2(110)$ surface (Fig. 1, step 4), the stabilization being in this case of -2.45 eV. Formally it corresponds to a Ce_2O_2 dimer adsorbed on the surface. The energy exchange for the whole process, i.e. direct transformation from steps 2 to 4, would be

as large as -10.48 eV. This highly exothermic process clearly implies that as long as "free" Ce atoms and monomers coexist on the surface, dimers will be formed from their interaction. The oxidation state for both Ce atoms in the dimer was Ce^{3+}. The process could be described as

$$CeO_2(Ce^{4+}) \text{ on } TiO_2 + Ce + 2Ti^{4+}(TiO_2)$$
$$\rightarrow Ce_2O_2(Ce^{3+}) \text{ on } TiO_2 + 2Ti^{3+}(TiO_2). \quad (3)$$

We will now consider the interaction of a Ce_2O_2 dimer with oxygen to form a dimer with a composition of Ce_2O_3 (Fig. 1, steps 4 and 5). It is well known that the presence of oxygen vacancies on $TiO_2(110)$ (which formally involves two Ti^{3+} cations/vacancy) generates adsorbed O atoms under oxygen pressure. After deposition of Ce atoms and formation of the first dimers we have generated Ti^{3+} species [see Eqs. (1) and (3)] which are able to dissociate oxygen. The presence of such adsorbed O atoms after Ce deposition under oxygen pressure were observed in STM images,[21] and prompted us to consider models with a extra atomic oxygen adsorbed on the surface. Indeed, the O atoms readily react with the surface reoxidizing Ti^{3+} centers and forming Ce_2O_3 dimer. The process could be described as

$$Ce_2O_2(Ce^{3+}) \text{ on } TiO_2 + 2Ti^{3+}(TiO_2) + \tfrac{1}{2}O_2$$
$$\rightarrow Ce_2O_3(Ce^{3+}) \text{ on } TiO_2. \quad (4)$$
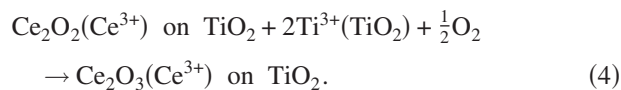
The energy that is released in this process is -2.59 eV and the structure obtained is reported in Fig. 1, step 5.

Let us now complete the oxidation of the system by adding an extra oxygen atom, i.e., the transformation from the Ce_2O_3 dimer to two CeO_2 monomers (Fig. 1, steps 5 and 6). As can be seen the process is exothermic but, in contrast to the previous oxidation step, (steps $4 \rightarrow 5$), the released energy amounts for only -0.92 eV (roughly one third). The reason for this is that now there are no longer high energy Ti 3d electrons but two electrons in relatively low energy Ce 4f states. Since the incoming O 2p states are lower in energy than the 4f, the electronic transfer process from 4f to 2p states is still favorable, but the released energy is much lower. This means that as long as Ti^{3+} species exist, O_2 will prefer to adsorb and dissociate on them because the stabilization energy for the system is much higher. Therefore, even though the oxidation process of dimers is favorable, it is not the preferred site for the adsorption and dissociation of O_2. In consequence, the oxidation of Ce_2O_3 will not happen until all the Ti^{3+} species completely disappear from the system. The process could be described as

$$Ce_2O_3(Ce^{3+}) \text{ on } TiO_2 + \tfrac{1}{2}O_2 \rightarrow 2CeO_2(Ce^{4+}) \text{ on } TiO_2. \quad (5)$$
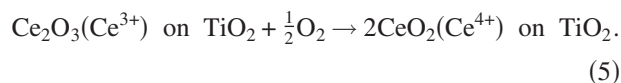
B. Formation energy and redox properties

The structures seen in Fig. 1 and in STM images[21] for the ceria clusters in contact with $TiO_2(110)$ are quite different from the fluorite structure characteristic of bulk CeO_2. Furthermore, the energetic analysis that we have discussed so far might appear surprising if we compare it with the same process in bulk. The energy involved in the oxidation process

TABLE I. Formation energies (eV) per Ce atom (see the text for details) of bulk and adsorbed-particle phases of CeO_2 and Ce_2O_3 species. The differences between the phases for each species and between the species for each phase are shown for easy measuring of the supported-particle effect on the formation energy (0.87 eV/Ce atom).

	Bulk	Particle on surface	ΔE (particle-bulk)
CeO_2	-14.50	-13.88	0.62
Ce_2O_3	-13.22	-13.47	-0.25
$\Delta E(Ce_2O_3-CeO_2)$	1.28	0.41	0.87

from Ce_2O_3 (bulk) to $2CeO_2$ (bulk) in the presence of $\tfrac{1}{2}O_2$ (g) is -2.56 eV (theory) and -3.95 eV (exp), respectively.[57] The fact that the oxidation is less favored when CeO_x NPs are supported on the $TiO_2(110)$ surface might arise from two possibilities: either Ce_2O_3 NPs are stabilized, or CeO_2 NPs are destabilized when they are deposited on the titania surface, and of course it may also due to a combination of both contributions. In order to try to quantify these effects we have estimated the formation energy for such mixed-metal oxide phases, and compared with the formation of the bulk phases. The formation energy (per Ce atom) for the bulk phase may be written as

$$\Delta E_f(CeO_x) = E(CeO_x) - E(Ce, atom) - \frac{x}{2}E(O_2, g)$$

and for the particles on the surface as

$$\Delta E_f(CeO_x) = E(CeO_x/TiO_2) - E(TiO_2, slab)$$
$$- E(Ce, atom) - \frac{x}{2}E(O_2, g),$$

where $E(CeO_x)$ is the bulk energy per Ce atom, $E(CeO_x/TiO_2)$ is the energy of the TiO_2 slab with a CeO_x particle adsorbed, $E(Ce, atom)$ is the energy of one Ce atom, $E(O_2, g)$ is the energy of the O_2 molecule, and $E(TiO_2, slab)$ is the energy of the TiO_2 slab. It is known that the formation energy is calculated with respect to the most stable phase (in this case we should use for Ce the energy from metallic bulk Ce per Ce atom). However, we are not interested in the exact values for the formation energy but in the difference among them, which is the same and not dependent on the reference energy for Ce. The results are shown in Table I.

The formation energy for a CeO_2 particle on the surface is lower (in absolute value) than for bulk CeO_2. It means that the particle would prefer to be as CeO_2 bulk rather than an isolated particle on $TiO_2(110)$. This is rather easy to understand, considering the reduction on coordination with the O atoms and the loss of Madelung energy. The instability introduced by the change in environment is 0.62 eV/Ce atom (see Table I). Instead, the Ce_2O_3 particle is stabilized on the surface with respect to the bulk by -0.25 eV/Ce atom (see Table I). Therefore, the combined effect of the Ce_2O_3 stabilization and the CeO_2 destabilization on the surface is the responsible for reducing the relative stability of CeO_2 and Ce_2O_3 from 1.28 eV/Ce atom in the bulk to 0.41 eV/Ce atom when in the form of a mixed-metal oxide on $TiO_2(110)$. Our calculations show that the destabilization of CeO_2 is significantly higher than the stabilization of Ce_2O_3 (see Table I).

TABLE II. Redox properties of the couple Ce_2O_3/CeO_2 measured through their reaction energies with CO/O_2 for supported particle and bulk phases. The difference in the reaction energy between both phases for each reaction is shown for easy measuring of the supported-particle effect.

		Particles (P)	Bulk (B)	Δ (P-B)
Oxidation	$Ce_2O_3 + \frac{1}{2}O_2 \rightarrow 2CeO_2$	−0.92	−2.56	1.64
Reduction	$2CeO_2 + CO \rightarrow Ce_2O_3 + CO_2$	−2.35	−0.71	−1.64

The fact that the formation energies of CeO_2 and Ce_2O_3 are similar in the case of a mixed-metal oxide (the difference is only 0.41 eV in 13.88 eV, i.e. 3%) means that the system is almost equally stabilized, on a per Ce atom basis, by the formation of CeO_2 monomers or Ce_2O_3 dimers. This result appears to be of great importance for catalysis on cerium oxides, as the $CeO_2 \leftrightarrow Ce_2O_3$ conversion has been found to play an essential role in many catalytic processes as the three-way car exhaust catalysis, SO_x destruction, alcohol synthesis from hydrogenation of CO or CO_2, and the water gas shift reaction.[58–60] There is evidence that in these cases CeO_2 does not only work as a support for different precious metals, but rather, due to its facile reducibility, ceria can also directly participate in different steps of the catalytic process. Its activity is precisely ascribed to its oxygen storage capacity,[58,60] i.e., easily taking up and releasing oxygen under oxidizing and reducing conditions, respectively, which takes place according to the formal reaction scheme: $2CeO_2 \rightarrow Ce_2O_3 + 0.5O_2$. Our calculations bring theoretical evidence that the energetic preference for this reaction can be related to the similarity of the formation energy of Ce^{3+} and Ce^{4+} species on the $TiO_2(111)$ substrate. It also suggests that we could easily tune the system to favor a given oxidation state, as the main final oxidation state will be determined by the specific conditions under which the reaction takes place, but not by the intrinsic nature of the Ce species. If the system reacts with reducing species the main final oxidation states will be Ce^{3+} while an oxidizing environment will lead the system to Ce^{4+}. So, if the oxygen storage capacity is high in the bulk phase, it will be even higher in the mixed-metal oxide phase at the nanometer level in the system CeO_x/TiO_2, what allows us to expect a higher catalytic activity than that of bare CeO_2. This has been shown for the WGS reaction case where the catalytic activity of $M/CeO_x/TiO_2$ (M=Au, Cu or Pt) was found to be more than two times higher than that of M/CeO_2 or M/TiO_2.[21,32]

To check the effect of environment on the $CeO_2 \leftrightarrow Ce_2O_3$ exchange, we have calculated the energies involved in the processes of oxidation of Ce_2O_3 with O_2 to give CeO_2, and reduction in CeO_2 with CO to give CO_2 and Ce_2O_3. Table II shows the energetics for both bulk ceria and CeO_x NPs supported on $TiO_2(110)$. In the bulk phase, it has been experimentally found that the oxidation process is strongly favored (−3.95 eV) while the reduction process by CO is not (the energy cost is 1.02 eV).[57] Our DFT calculations show a similar trend: the oxidation is more favored than the reduction (−2.56 eV versus −0.71 eV). We can see in Table II that the tendency in the mixed-metal oxide phase at the nanometer level is just the opposite than in bulk phase.

The reduction by CO is now clearly more favored (−2.35 eV) than the oxidation (−0.92 eV). Therefore, an inversion of the oxidation-reduction tendency of the system takes place when we move from bulk to CeO_x particles supported on TiO_2. At the nanometer level the mixed-metal oxide effect on the redox properties of the couple $Ce_2O_3/2CeO_2$ could be estimated to be 1.64 eV, as the reduction process is favored by −1.64 eV and the oxidation hampered by 1.64 eV with respect to the bulk (see Table II). Our conclusion that to reduce Ce^{4+} to Ce^{3+} is easier for the mixed-metal oxide, was confirmed by comparing the behavior of $CeO_2(111)$ and $CeO_x/TiO_2(110)$. For example, a $CeO_2(111)$ surface did not undergo reduction under an atmosphere of 20 Torr of CO at 400 K, while a $CeO_2/TiO_2(110)$ surface under the same conditions was completely transformed into $Ce_2O_3/TiO_2(110)$.[21]

C. TiO_x versus CeO_x particles on $TiO_2(110)$

In a recent article the formation of TiO_x clusters on the TiO_2 surface, formed by direct interaction of O_2 with interstitials Ti atoms which move from the bulk to the surface, has been reported.[33] To compare the behavior of CeO_x and TiO_x species on TiO_2 we report in Fig. 1 the adsorption-oxidation path for Ti. As can be seen the M^{4+} states (where M is the metal) are more stable for Ti than for Ce (Fig. 1, steps 2 and 6). In contrast, the M^{3+} states are always more stable with Ce than with Ti (Fig. 1, steps 1, 3–5). The difference is due to the higher energy of the $3d$ Ti^{3+} valence electron (see Fig. 2), while for Ce^{3+} the $4f$ electron is in a significantly lower level. In this case, the Ce center is neither greatly destabilized by forming Ce^{3+} nor greatly stabilized when moves to Ce^{4+}. This is in contrast to Ti, which is relatively more destabilized when reduced to Ti^{3+} and, consequently, the stabilization is much higher when it is reoxidized to Ti^{4+}. This makes the oxidation step from supported Ti_2O_3 to TiO_2 in O_2 presence much more favored −3.23 eV than the same step in the case of Ce (−0.92 eV) (see Fig. 1, steps 5→6). It also explains that the reduction from supported TiO_2 to Ti_2O_3 in the presence of CO is almost thermoneutral (−0.04 eV), while the same step in the case of supported ceria is neatly exothermic −2.35 eV.

D. Electronic structure and the relative stability

Overall, our calculations show that Ce_2O_3 is stabilized as mixed-metal oxide on the surface of TiO_2 compared to the bulk phase, while CeO_2 is destabilized. As a result, the TiO_2-supported ceria cluster can be oxidized or reduced in a much easier way than the bulk materials. To better understand the different stability between these phases, we have calculated the DOS projected on Ce and O atoms in both bulk and supported-particle phases for Ce_2O_3 and CeO_2. Here, the DOS for the isolated free particle with the same geometry that the supported particle has also been included for comparison, in order to determine the effect of the structure of the NP and the effect of the interaction with the support. As shown in Fig. 3, the formation of the mixed-metal oxide involves significant changes in the electronic structure. For the free particle, molecular bands with strongly mixed Ce $4f$ and O $2p$ were observed, indicating a high degree of
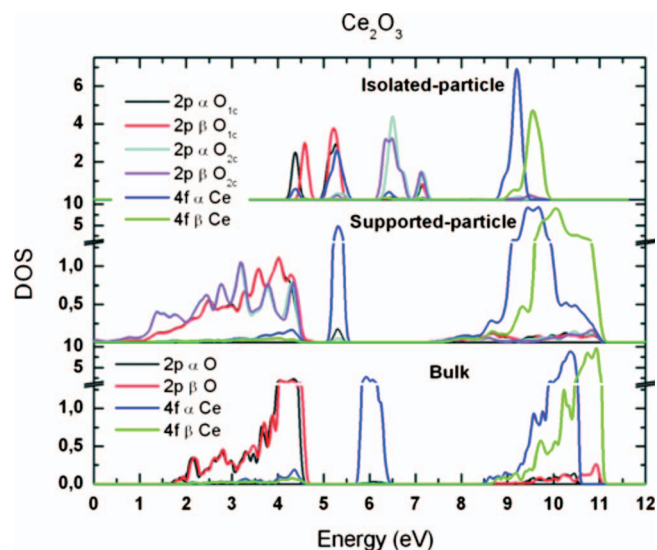
FIG. 3. DOS projected on Ce and O atoms of the Ce_2O_3 unit for the systems: perfect bulk (bottom), supported particle on $TiO_2(110)$ (middle), and isolated particle with the same geometry than that of the supported one (top). O_{1c} and O_{2c} stand for oxygen atoms mono- and bi-coordinated to Ce atoms respectively.

FIG. 4. DOS projected on Ce and O atoms of the CeO_2 unit for the systems: perfect bulk (bottom) and supported particle on $TiO_2(110)$ (top).

covalency. That is, the isolated Ce_2O_3 unit is electronically transformed into a molecule. However, when this particle is deposited on TiO_2, the electronic structure of the particle returns to a solidlike DOS with wide O $2p$ and Ce $4f$ bands (see Fig. 3).The effect of the interaction with the support is very important since it "crystallizes" the electronic structure of the cerium oxide particle from an initial "molecular" distribution, leading to a true mixed-metal oxide rather than a supported particle.

Compared to bulk Ce_2O_3, the $2p$ and $4f$ main bands are wider in the nanomixed-metal oxide. As a consequence, after deposition, the band-gap between the top of the O $2p$ band and the bottom of the main Ce $4f$ band is reduced by 1.44 eV. In addition, the Ce $4f$ band, that corresponds to the valence electron of the reduced specie Ce^{3+} and locates in the midband gap between the main O $2p$ and the conduction bands, is shifted by 0.8 eV to the lower energies in the mixed-metal oxide. In other words, the $4f$ valence electron of Ce^{3+} is stabilized with respect to bulk phase. As shown in Fig. 3, there is almost no gap between the O $2p$ band and $4f$ Ce^{3+} little band in the mixed-metal oxide. This close distribution allows a higher mixing between the two bands, and therefore increases the covalent character of the bond. In fact, we can see in Fig. 3 that O $2p$ band appears at the same energy as Ce^{3+} $4f$ band, indicating a certain covalent character of the Ce–O bond in the particle. In contrast, the Ce–O overlapping is, however, much lower in the bulk phase. Furthermore, the width of the little $4f$ peak of Ce^{3+} is also reduced by 0.25 eV when going from bulk to surface nanomixed-metal oxide, indicating a more localized molecular feature (approaching a single level energy like in the molecules) with respect to the bulk. That is, the Ce_2O_3 unit seems to be crystallized by the interaction with the support, but some covalent character coming from the molecular electronic structure of the isolated particle remains in the sup-
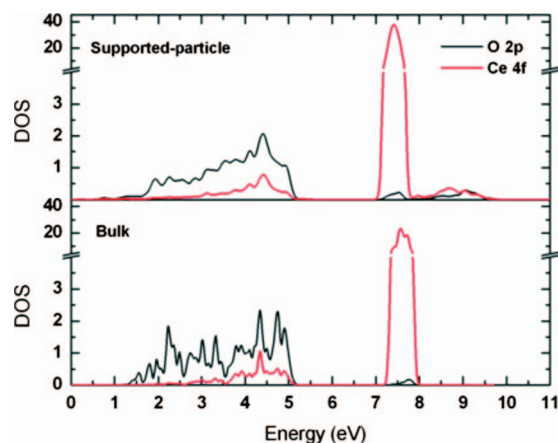
ported particle. This remaining covalency helps stabilizing the supported Ce_2O_3 unit by lowering the energy of the Ce^{3+} $4f$ band.

As the $4f$ band of fully oxidized Ce^{4+} is completely empty no electronic-induced change in the energy is expected by the interaction with the support. Indeed, no significant differences are observed when the DOS of the supported CeO_2 unit and that of the bulk are compared (Fig. 4). Therefore, there is no electronic stabilization in the CeO_2 unit when going from bulk to surface nanomixed-metal oxide. Accordingly, the loss of the Madelung potential and coordination with O atoms is not electronically compensated, and CeO_2 is more stable as bulk phase than as nanomixed-metal oxide on the TiO_2 surface.

E. Adsorption and dissociation of H_2O on $CeO_x/TiO_2(110)$

As stated in Sec. I, all the steps involved in the WGS reaction can take place on the surfaces of the plain metals or metal NPs, but for the dissociation of H_2O a high activation barrier has been predicted.[24,25] In contrast, water easily dissociates on the metal oxide, therefore, an adequate coupling of the oxide and metal properties leads to a high active catalyst. That is why Au/TiO_2 or Cu/TiO_2 are efficient WGS catalysts.[22] The activation energy for the dissociation of H_2O on TiO_2 oxygen vacancies has been calculated to be 0.35 eV (Ref. 27) while on the (111) surface of Au and Cu the barrier increases to 1.95 eV (Ref. 61) and 1.36 eV,[62] respectively. Although, the presence of steps in the metal surfaces can decrease the activation energy for the dissociation of H_2O on Cu from 1.36 eV in Cu(111) to 0.9 eV (or 0.71 eV with the zero-point correction) in Cu(321),[63] the activation energy is still twice the activation barrier in the $TiO_2(110)$ oxygen vacancy. Therefore, any oxide, which decreases the barrier for the dissociation of H_2O, is expected to improve the catalytic activity of the system M/MO_x (where M is a metal). Since we have shown that the $Au/CeO_x/TiO_2$ system is three times more active than Au/TiO_2 for the WGS reaction and four times more active than Cu/ZnO, the most common WGS catalyst used in the industry,[21] it has been postulated that the barrier for the water dissociation on the CeO_x par-
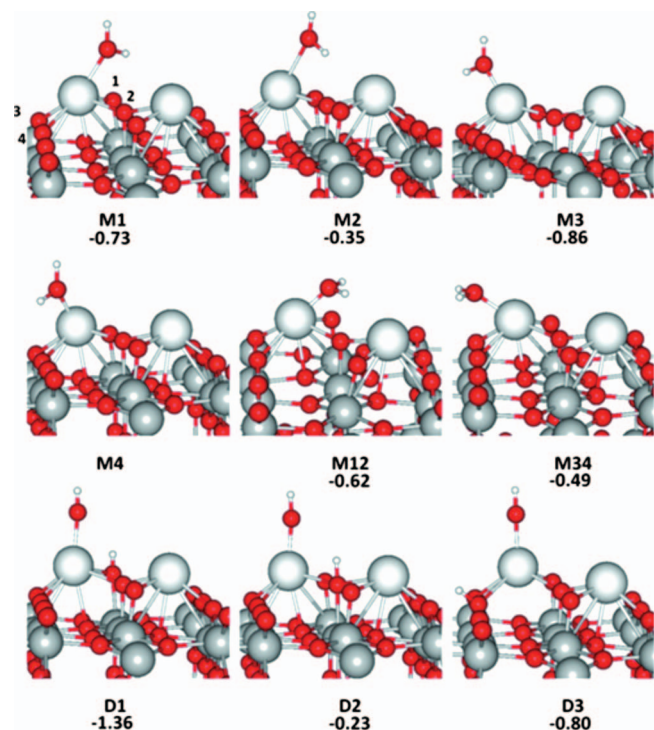
FIG. 5. Adsorption sites, geometries, and adsorption energies (eV) for the dissociation of water on $Ce_2O_3/TiO_2(110)$. In order to simplify the view only the Ce_2O_3 particle and water are shown in the figure. The nonequivalent oxygen atoms have been labeled as: 1, 2, 3, and 4. Atom colors: red (O), dark gray (Ti), white (big spheres, Ce) and white (small spheres, H).
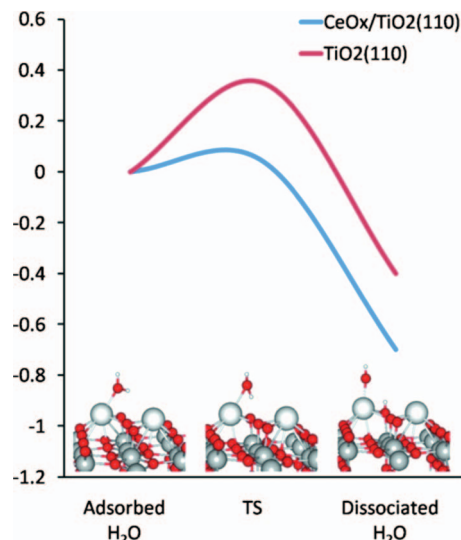

FIG. 6. Energy pathway for the dissociation of a H_2O molecule on $Ce_2O_3/TiO_2(110)$ (our calculations) and on an oxygen vacancy of $TiO_2(110)$ (Ref. 27). Initial and final geometries for the dissociation on $Ce_2O_3/TiO_2(110)$ are shown. While for reduced $TiO_2(110)$ surface the reaction energy is ~ -0.4 eV with an activation barrier of 0.35 eV, for $Ce_2O_3/TiO_2(110)$ the reaction energy is more exothermic (-0.7 eV) with an activation barrier of only 0.04 eV. For atom colors see Fig. 5.

ticles will be smaller than on TiO_{2-x}. With the aim to confirm this aspect we report here an energetic analysis for the dissociation of water on $CeO_x/TiO_2(110)$.

To begin our analysis we examined the adsorption of a water molecule in the molecular and dissociated forms. Two different orientations were taken into account in which water can establish one or two hydrogen bonds (Fig. 5). Labels M and D refer to molecularly and dissociatively adsorbed water molecules, while the numbers indicate the oxygen atom to which is bound through hydrogen bond. Results for adsorption energies are reported in Fig. 5. For the molecular case, the larger interaction energy is -0.86 eV (site M3), although there is another site, (M1) slightly less favored (-0.73 eV). However, in the case of dissociated water there is a clear preference for site D1, where the transferred hydrogen binds oxygen O1 (see Fig. 5) that is the one with lower coordination, and therefore, the one with larger basicity. Given that the D1 site is by far the most stable, we considered a path for the water dissociation process, that may be easily visualized as the cleavage of an O–H bond starting from the configuration corresponding to M1 (Fig. 6). The transition state search using the CI-NEB algorithm showed an activation barrier of only 0.04 eV, i.e., eight times smaller than that found in the TiO_2 oxygen vacancy (see Fig. 6).[27] Moreover, the reaction energy for the dissociation of water on CeO_x/TiO_2 was found to be -0.70 eV, while on the oxygen vacancies of TiO_2 the estimated value was ~ -0.4 eV. These results unambiguously indicate the larger ability of CeO_x/TiO_2 to dissociate water and, therefore, can help to explain the superior WGS catalytic activity of the $M/CeO_x/TiO_2$ (M = Au, Cu, Pt) systems over M/TiO_2.[21,32]

IV. SUMMARY AND CONCLUSIONS

In this paper we report a theoretical study of the structural and electronic properties of CeO_x species supported on the rutile $TiO_2(110)$ surface by means of periodic GGA density-functional calculations that include a Hubbard-like correction U_{eff}. Deposition of Ce followed by reaction with O_2 gives rise to the formation of Ce_2O_3 dimers diagonally arranged on the $TiO_2(110)$ surface, in agreement with the experimental observations. The redox properties of these CeO_x NPs haven been analyzed and found to be quite different from those of bulk ceria. Thus, the reduction process: $2CeO_2 + CO \rightarrow Ce_2O_3 + CO_2$ is favored over the oxidation reaction: $Ce_2O_3 + (1/2)O_2 \rightarrow 2CeO_2$. Moreover, while, as expected, the CeO_2 species are less stable as supported NPs on $TiO_2(110)$ than as bulk, the Ce_2O_3 species are stabilized when they are supported. These results suggest that the CeO_x/TiO_2 interface behaves like a mixed-metal oxide rather than a supported NP of CeO_x, and that this mixed-metal oxide favors the +3 oxidation state over the +4 under WGS reaction conditions. This is in contrast to the behavior of the $TiO_x/TiO_2(110)$ system, for which our calculations show that the reduced state Ti^{3+} is not favored over the Ti^{4+}. This difference is obviously due to the fact that the $3d$ occupied states in Ti^{3+} are significantly higher in energy than the $4f$ states of Ce^{3+}, and as a result, under WGS reaction conditions, a full oxidation of Ti is expected, with loss of the potential activity of Ti^{3+} centers.

The effect of a mixed-metal oxide at the nanometer level on the WGS catalytic activity has been analyzed by studying the interaction of the $CeO_x/TiO_2(110)$ system with water. The dissociation process is quite exothermic, -0.70 eV, while the activation energy for the dissociation is estimated to be as small as 0.04 eV. This is in contrast to a common support widely used in these reactions, namely TiO_2, for

which the barrier for the dissociation in an oxygen vacancy has been calculated to be 0.35 eV.[27] This larger ability of CeO_x/TiO_2 to dissociate water may help to explain the superior WGS catalytic activity of the $M/CeO_x/TiO_2$ (M = Au, Cu, Pt) systems over M/TiO_2.[21,32]

[1] N. Kruse, A. Frennet, and J. -M.Bastin, Top. Catal. **16/17**, 1 (2001).

[2] D. E. Webster, Top. Catal. **16/17**, 33 (2001).

[3] *Recent Advances in Catalysis for Hydrogen Production and Fuel Processing for Fuel Cells*, edited by C. Song (Springer Science + Business Media, Luxembourg), Top Catal. 49, 1–24 (.2008).

[4] *Catalysis by Gold*, edited by G. J. Hutchings and D. W. Goodman (Springer Science + Business Media, Luxembourg), 44, 1–343 (2007).

[5] *Catalysis by Gold*, edited by G. J. Hutchings and M. Haruta (Elsevier, Amsterdam), Appl. Catal. A: Gen. 291, 1–262 (2005).

[6] R. Burch, Phys. Chem. Chem. Phys. **8**, 5483 (2006).

[7] O. Thinon, F. Diehl, P. Avenier, and Y. Schuurman, Catal. Today **137**, 29 (2008).

[8] M. Haruta, N. Yamada, T. Kobayashi, and S. Ijima, J. Catal. **115**, 301 (1989).

[9] M. Valden, X. Lai, and D. W. Goodman, Science **281**, 1647 (1998).

[10] M. S. Chen and D. W. Goodman, Science **306**, 252 (2004).

[11] Q. Fu, H. Saltsburg, and M. Flytzani-Stephanopoulos, Science **301**, 935 (2003).

[12] J. A. Rodriguez, P. Liu, J. Hrbek, J. Evans, and M. Perez, Angew. Chem., Int. Ed. **46**, 1329 (2007).

[13] J. Guzman, S. Carrettin, J. C. Fierro-Gonzalez, B. C. Gates, and A. Corma, Angew. Chem., Int. Ed. **44**, 4778 (2005).

[14] W. Deng and M. Flytzani-Stephanopoulos, Angew. Chem., Int. Ed. **45**, 2285 (2006).

[15] R. Si and M. Flytzani-Stephanopoulos, Angew. Chem., Int. Ed. **47**, 2884 (2008).

[16] M. S. Chen and D. W. Goodman, Top. Catal. **44**, 41 (2007).

[17] C. T. Campbell and C. H. F. Peden, Science **309**, 713 (2005).

[18] F. Esch, S. Fabris, L. Zhou, T. Montini, C. Africh, P. Fornasiero, G. Comelli, and R. Rosei, Science **309**, 752 (2005).

[19] S. Torbrügge, M. Reichling, A. Ishiyama, S. Morita, and O. Custance, Phys. Rev. Lett. **99**, 056101 (2007).

[20] J. A. Rodriguez, S. Ma, P. Liu, J. Hrbeck, J. Evans, and M. Perez, Science **318**, 1757 (2007).

[21] J. B. Park, J. Graciani, J. Evans, D. Stacchiola, S. Ma, P. Liu, A. Nambu, J. F. Sanz, J. Hrbek, and J. A. Rodriguez, Proc. Natl. Acad. Sci. U.S.A. **106**, 4975 (2009).

[22] J. A. Rodríguez, J. Evans, J. Graciani, J. B. Park, and J. F. Sanz, J. Phys. Chem. C **113**, 7364 (2009).

[23] J. A. Rodriguez, J. Graciani, J. Evans, J. B. Park, F. Yang, D. Stacchiola, S. D. Senanayake, S. Ma, M. Pérez, P. Liu, J. F. Sanz, and J. Hrbek, Angew. Chem., Int. Ed. **48**, 8047 (2009).

[24] A. A. Phatak, W. N. Delgass, F. H. Ribeiro, and W. F. Schneider, J. Phys. Chem. C **113**, 7269 (2009).

[25] P. Liu and J. A. Rodriguez, J. Chem. Phys. **126**, 164705 (2007).

[26] M. A. Henderson, Surf. Sci. Rep. **46**, 1 (2002).

[27] J. Oviedo, R. Sanchez-de-Armas, M. A. San Miguel, and J. F. Sanz, J. Phys. Chem. C **112**, 17737 (2008).

[28] T. Wu, W. E. Kaden, and S. L. Anderson, J. Phys. Chem. C **112**, 9006 (2008).

[29] G. Ketteler, S. Yamamoto, H. Bluhm, K. Andersson, D. E. Starr, D. F. Ogletree, H. Ogasawara, A. Nilsson, and M. Salmeron, J. Phys. Chem. C **111**, 8278 (2007).

[30] S.-C. Li, Z. Zhang, D. Sheppard, B. D. Kay, J. M. White, Y. Du, I. Lyubinetsky, G. Henkelman, and Z. Dohnalek, J. Am. Chem. Soc. **130**, 9080 (2008).

[31] S. Kajita, T. Minato, H. S. Kato, M. Kawai, and T. Nakayama, J. Chem. Phys. **127**, 104709 (2007).

[32] J. B. Park, J. Graciani, J. Evans, D. Stacchiola, S. D. Senanayake, L. Barrio, P. Liu, J. F. Sanz, J. Hrbek, and J. A. Rodriguez, J. Am. Chem. Soc. **132**, 356 (2010).

[33] S. Wendt, P. T. Sprunger, E. Lira, G. K. H. Madsen, Z. Li, J. Ø. Hansen, J. Matthiesen, A. Blekinge-Rasmussen, E. Lægsgaard, B. Hammer, and F. Besenbacher, Science **320**, 1755 (2008).

[34] G. Kresse and J. Joubert, Phys. Rev. B **59**, 1758 (1999).

[35] J. Perdew, J. Chevary, S. Vosko, K. Jackson, M. Pederson, D. Singh, and C. Fiolhais, Phys. Rev. B **46**, 6671 (1992).

[36] G. Kresse and J. Hafner, Phys. Rev. B **47**, 558 (1993).

[37] G. Kresse and J. Furthmüller, Comput. Mater. Sci. **6**, 15 (1996); Phys. Rev. B **54**, 11169 (1996).

[38] K. J. Hameeuw, G. Cantele, D. Ninno, F. Trani, and G. Iadonesi, J. Chem. Phys. **124**, 024708 (2006).

[39] S. J. Thompson and S. P. Lewis, Phys. Rev. B **73**, 073403 (2006).

[40] J. Graciani, A. Nambu, J. Evans, J. A. Rodriguez, and J. F. Sanz, J. Am. Chem. Soc. **130**, 12056 (2008).

[41] J. Graciani, L. J. Álvarez, J. A. Rodriguez, and J. F. Sanz, J. Phys. Chem. C **112**, 2624 (2008).

[42] S. L. Dudarev, G. A. Botton, S. Y. Savrasov, C. J. Humphreys, and A. P. Sutton, Phys. Rev. B **57**, 1505 (1998).

[43] S. Fabris, S. de Gironcoli, S. Baroni, G. Vicario, and G. Balducci, Phys. Rev. B **72**, 237102 (2005).

[44] M. Cococcioni and S. de Gironcoli, Phys. Rev. B **71**, 035105 (2005).

[45] C. W. M. Castleton, J. Kullgren, and K. Hermansson, J. Chem. Phys. **127**, 244704 (2007).

[46] D. A. Andersson, S. I. Simak, B. Johansson, I. A. Abrikosov, and N. V. Skorodumova, Phys. Rev. B **75**, 035109 (2007).

[47] M. Nolan, S. Grigoleit, D. C. Sayle, S. C. Parker, and G. W. Watson, Surf. Sci. **576**, 217 (2005).

[48] M. Nolan, S. C. Parker, and G. W. Watson, Surf. Sci. **595**, 223 (2005).

[49] M. Nolan, S. C. Parker, and G. W. Watson, J. Phys. Chem. B **110**, 2256 (2006).

[50] M. B. Watkins, A. S. Foster, and A. L. Shluger, J. Phys. Chem. C **111**, 15337 (2007).

[51] Z. Yang, Z. Lu, and G. Luo, Phys. Rev. B **76**, 075421 (2007).

[52] J. L. F. Da Silva, Phys. Rev. B **76**, 193108 (2007).

[53] J. L. F. Da Silva, M. V. Ganduglia-Pirovano, J. Sauer, V. Bayer, and G. Kresse, Phys. Rev. B **75**, 045121 (2007).

[54] C. Loschen, J. Carrasco, K. M. Neyman, and F. Illas, Phys. Rev. B **75**, 035115 (2007).

[55] C. Loschen, A. Migani, S. T. Bromley, F. Illas, and K. M. Neyman, Phys. Chem. Chem. Phys. **10**, 5730 (2008).

[56] G. Henkelman, B. Uberuaga, and H. Jonsson, J. Chem. Phys. **113**, 9901 (2000).

[57] D. R. Lide, *CRC Handbook of Chemistry and Physics*, 87th ed. (CRC, Cleveland, 2006).

[58] A. Trovarelli, Catal. Rev. - Sci. Eng. **38**, 439 (1996).

[59] M. Shelef and R. W. McCabe, Catal. Today **62**, 35 (2000).

[60] A. Trovarelli, *Catalysis by Ceria and Related Materials*, 1st ed. (World Scientific, Singapore, 2002).

[61] S. Kandoi, A. A. Gokhale, L. C. Grabow, J. A. Dumesic, and M. Mavrikakis, Catal. Lett. **93**, 93 (2004).

[62] A. A. Gokhale, J. A. Dumesic, and M. Mavrikakis, J. Am. Chem. Soc. **130**, 1402 (2008).

[63] J. L. C. Fajín, M. N. D. S. Cordeiro, F. Illas, and J. R. B. Gomes, J. Catal. **268**, 131 (2009).